Enhanced boron doping of thin diamond films grown in deuterium-rich microwave plasma

R. Bogdanowicz[1*], M. Sobaszek[1], M. Sawczak[2], G.M.Grigorian[3], M. Ficek[1], P. Caban[4], A. Herman[5] and A.Cenian[2]

[1]*Department of Metrology and Optoelectronics, Faculty of Electronics, Telecommunications and Informatics, Gdańsk University of Technology, 11/12 Narutowicza St., 80-233 Gdańsk, Poland*

[2]*Institute of Fluid Flow Machinery, Polish Academy of Sciences, 80-231 Gdańsk, 14 Fiszera St, Poland*

[3]*St. Petersburg State University, 199034, St. Petersburg, Russia*

[4]*Institute of Electronic Materials Technology, 133 Wolczynska St., 01-919 Warsaw, Poland*

[5]*Department Department of Inorganic Chemistry, Chemical Faculty, Gdańsk University of Technology, 11/12 Narutowicza St, 80-233 Gdańsk, Poland*

Abstract. The boron-doped diamond thin films were growth in deuterium rich microwave plasma in CVD process. The mechanism of influence of plasma composition on boron doping level was studied using optical emission spectroscopy. Deuterium rich plasma results in an increased dissociation of B_2H_6 precursor and intense boron-radicals' production. In consequence, a higher doping level of diamond films was observed by means of Laser Induced Breakdown Spectroscopy and Raman spectroscopy. Deuterium species modify the mechanism of boron incorporation into thin films leading to increased boron concentration. Lower concentrations of sp^2 phases and CH defects have been noticed in the films deposited in the plasma with deuterium than with hydrogen. Moreover, all BH_x (x = 0–3) species can bind to radical sites on the diamond {100} surface to form stable complexes. The enhanced boron doping is attributed to the lower energy of B-H bond at the growth surface, when compared to C-H bond. The hydrogen abstraction from B-H site is providing dangling bond for diamond growth and boron incorporation. This effect plays a main role due to extended dissociation caused by deuterium rich plasma. The increase in the carrier concentration and the decrease in the Hall mobility for the BDD samples grown in deuterium was registered.

Keywords: microwave plasma-assisted chemical vapour deposition; optical emission spectroscopy; boron-doped diamond; Hall Effect; Raman spectroscopy

*Corresponding author: E-mail: rbogdan@eti.pg.edu.pl (*Robert Bogdanowicz*); Tel.: +48-58-347-15-03; Fax: +48 58-347-18-48

1. Introduction

Boron-doped diamond (BDD) tend to be grown mostly from the gas phase by microwave plasma-assisted chemical vapour deposition (MW PACVD) [1] or from hot filament chemical-vapour depositions (HFCVD) [2]. The growth and design of boron-doped diamond surfaces with outstanding characteristics of surface quality, chemical and electronic properties have attracted much attention [3–6]. It is worth noting that only a small fraction (~0.2%) of boron acceptors are ionized at room temperature due to the high bonding energy. For single-crystal diamond, the metal-insulator transition has been reported by Lagrange et al. [10], Klein et al. [7] or Kawano et al. [8] and more recently by Bousquet et al. [9]. Since the boron dopant is situated between 2 and 5×10^{20} atoms cm^{-3} the diamond undergoes a transition from p-type semiconducting to metallic, where conduction is dominated by temperature-independent carrier concentration with mainly nearest-neighbor hopping conduction [9].

Various approaches have been investigated by numerous research groups to enhance boron doping, leading to improved electronic properties (e.g., carrier mobility, wide-bandgap). The variety of experimental studies of chemical vapour deposition (CVD) processes for the deposition of BDD films have been described, using various gas composition, temperature, etc. [4]. Wang *et al.* [10] reported heavily boron-doped nanocrystalline diamond films produced from Ar-rich or H_2-rich source-gas mixtures results in equivalent electrical and electrochemical properties. Issaoui *et al.* [11] showed that the microwave power density is one of the key factors allowing tuning doping efficiencies over two orders of magnitude. Low resistance (~1 Ohm-cm) homoepitaxial diamond (100)-films were grown by Teraji *et al.* [12] using high-power MW PACVD and High Pressure and High-Temperature type-Ib (100) diamond single-crystals substrates. In the case of single-crystal diamond films, the high-power conditions are responsible for enhanced (of about one order of magnitude) boron-incorporation efficiency resulting in carrier concentration of 6×10^{15} cm^{-3}.

Several attempts to replace H_2 with deuterium D_2 in the CVD diamond growth have been reported to date. Chevallier *et al.* [13] investigated the (111) n-type homoepitaxial diamond phosphorus-doped films grown from a $CH_4{:}D_2$ mixture. The diamond films were grown using $CH_4{:}H_2$ mixture usually shows in Raman or Fourier Transform Infrared spectra hydrogen-related local vibrational modes corresponding to $C–CH_x$ present at the intergrain regions [14,15]. These defects completely disappear under the replacement of hydrogen by deuterium in the gas mixture [13,16]. Next, hydrogen is a relatively fast diffuser in a boron-doped diamond because it migrates as a proton, which is known to have low migration energy (0.1–0.2 eV). During this diffusion, protons are trapped

by boron acceptors giving rise to (B,H) complexes and to passivation of boron acceptors by hydrogen [17].

Moreover, suppression of point defects in the non-epitaxial crystallites, and an increase of free-exciton emission-intensity was revealed by Mizuochi *et al.* [18] in a deuterium-rich microwave plasma. The *ca.* 30 % higher etching rate of diamond by deuterium vs. hydrogen was also demonstrated. Ternyak *et al.* [19] grew HFCVD diamond films using $CD_4 + D_2$ gas mixtures. The D_2 molecule is responsible for the larger and more faceted grain grown in HFCVD since the thermally activated deuterium tends to etch away non-diamond species more effectively than the hydrogen species [20].

Besides, the phenomenon of deuterium diffusion in BDD was extensively reported for radio frequency [21] or microwave excited plasmas [22]. It was demonstrated [23], that the grain size of the polycrystalline diamond is the key parameter for efficient deuterium diffusion and trapping on boron atoms. The hole concentration decreases, while the Hall mobility increases up to 120 cm^2 V^{-1} s^{-1} mainly due to the passivation of boron acceptors in a polycrystalline diamond [23]. Since the deuterium-diffusion experiments were performed in the post-growth mode, these effects are depth limited and confined by interactions in the BDD molecular structure.

Here we report extensive comparative studies of the main species in microwave plasma by optical emission spectroscopy (C_2, CH, BH, H_x, and H_2) and morphology and composition of boron-doped diamond films. To the best of our knowledge, the effects of replacing large volume of hydrogen by deuterium during BDD growth in microwave plasma have not been reported up to now. The plasma parameters, i.e., plasma composition as functions of input power of microwave and deuterium admixture were investigated and discussed. The grown boron-doped CVD diamond-films from hydrogenated and deuterated gas mixtures was studied by Raman spectroscopy and Laser Induced Breakdown Spectroscopy (LIBS), while the resistivity and Hall effect measurements were performed for their electrical characterization.

2. Experimental

2.1. Optical emission studies of $D_2/CH_4/B_2H_6$ and $H_2/CH_4/B_2H_6$ plasma

Diamond-film growth and plasma investigation by Optical Emission Spectroscopy (OES) was carried out in MW PACVD process (SEKI Technotron AX5400S, Japan). The optical-emission spectra were recorded in the experimental setup presented in Figure 1. The plasma emission was collected with a quartz lens located at the front of a quartz chamber window and focused on the optical-fiber entrance. The fiber, located in the lens image plane, was mounted on the XY stage and moved

perpendicular to the lens optical axes to select a plasma zone for recording the emission spectrum. The radiation was collected from the plasma volume 3 – 5 mm above the sample surface. The detection of plasma emission was realized using 0.3 m monochromator (SR303i, Andor, United Kingdom) equipped with 1200 grooves/mm grating and intensified charge-coupled device (i-CCD) detector (DH740, Andor, United Kingdom). Spectra were recorded in the range of 200 – 800 nm. Each presented spectrum was averaged from 1000 acquisitions.
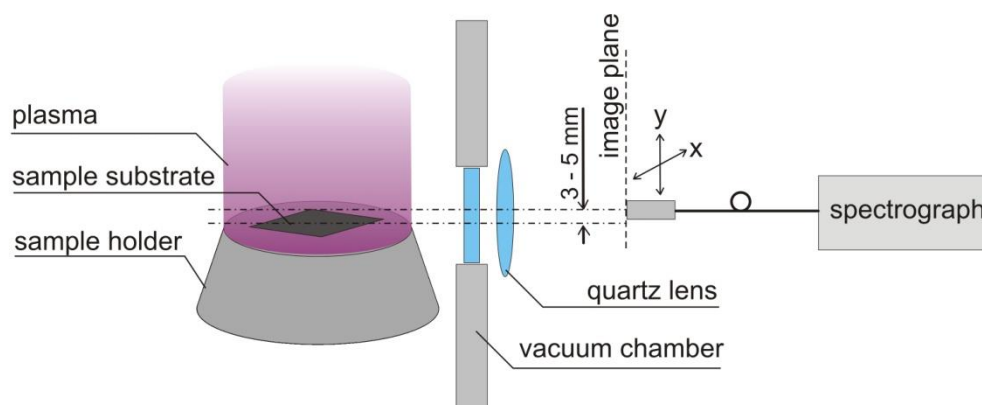

Figure 1. Experimental setup for plasma optical emission measurements.

The high-frequency discharge in D_2/CH_4 and H_2/CH_4 mixture with a small addition of B_2H_6 was studied. A series of important processes leading to excitation and dissociation of mixture components, and appearance of many radicals and excited and ground states atomic species and molecules, is taking place.

2.2. The growth of thin diamond films in $D_2/CH_4/B_2H_6$ and $H_2/CH_4/B_2H_6$ plasma

The diamond films (BDD_D and BDD_H) were deposited on p-type (100) silicon and fused silica glass substrates (1 x 1 cm^2). All substrates were cleaned in acetone in ultrasonic bath for 5 minutes, next were washed in 2-propanol. The substrates were sonicated in nanodiamond suspension containing diamond particles 4-5 nm suspended in dimethyl sulfoxide (BlueSeeds, Adámas Nanotechnologies, USA). D_2/CH_4 and H_2/CH_4 gas mixture of 1% vol. with the overall gas flow of 300 sccm and temperature of 700°C was used. The films presented in the results section was grown at pressure of 6.7 kPa and $P_{MW} = 1300$ W of microwave power resulting in the high-density direct plasma at the region of the substrate. The grounded substrate is immersed in plasma inducing direct plasma diamond growth and etching non-diamond phases. The high density of plasma delivers rapid dissociations of important growth species. Diborane (B_2H_6) was used as a boron dopant precursor. The boron doping level expressed as the [B]/[C] ratio in the gas phase was set to 10k ppm. The growth

4

time of BDD_D films was 2 hours, producing sub-microcrystalline films with an average thickness of 200 nm. In the case of BDD_H films, the growth time was 1 hour to achieve a similar film thickness. The non-conductive fused silica substrates were applied for electrical parameters studies.

2.3. Diamond film analysis techniques

LIBS spectra were recorded using a laboratory-built system consisting of Nd:YAG laser (Briliant B, Quantel) used as an excitation source for laser ablation and detection system equipped with 0.3 m monochromator (SR303i, Andor) with 1200 grooves/mm grating and ICCD detector (DH740, Andor). The laser beam (1064 nm, 6 nm pulse duration) was focused on a sample surface using a quartz lens (f=300mm). Beam energy was tuned to optimize the ablation rate and LIBS signal for thin 0.3 μm BDD film. LIBS spectra were averaged over 100 measurements performed for each sample. Because BDD film was evaporated during a single laser pulse, the sample was moved after each laser pulse by a distance of 100 μm, comparable to the laser beam-spot diameter. Raman measurements were carried out by means of a micro Raman system (InVia, Renishaw) equipped with 514 nm argon-ion laser as an excitation source. The thickness of the samples was also studied by stylus profilometer (Veeco Dektak, USA).

Spectroscopic ellipsometry (SE) investigations were carried out with a phase-modulated ellipsometer Jobin-Yvon UVISEL (HORIBA Jobin-Yvon Inc., Edison, USA). The investigated wavelength region was 250–800 nm with a step of less than 0.5 nm. The experiments were carried out at room temperature using an angle of incidence fixed at 70°, and the compensator was set at 45°. The light spot size was 2 mm in diameter. The incidence angle resulted from Brewster's angle of the silicon substrate. DeltaPsi software (v. 2.4.3) was used to determine the spectral distributions of refractive index $n(\lambda)$ and the extinction coefficient $k(\lambda)$ of the diamond films.

The Hall effect and resistivity measurements were carried out by the Van der Pauw method at room temperature at diamond films deposited on fused silica substrates. The 0.55T Ecopia HMS-3000 Hall effect setup was utilized for Hall effect characterization. The four holder probes were placed in the four corners of each 10 mm x 10 mm substrate. The Ti/Pt/Au ohmic contacts were deposited at four points located symmetrically on each diamond surface with the help of a mechanical mask beforehand. The capacitance-voltage (C–V) measurements with Al Schottky contacts were utilized to confirm the acceptor concentration of the boron-doped samples.

3. Results and discussion

3.1. Optical emission spectra of microwave plasmas in $D_2/CH_4/B_2H_6$ and $H_2/CH_4/B_2H_6$ mixtures

5

In order to determine the role of deuterium in plasma and its relation to film quality, emission spectra of microwave plasma in $D_2/CH_4/B_2H_6$ and $H_2/CH_4/B_2H_6$ mixtures were investigated. The spectral feature related to H_2/D_2 Fulcher system ($d^3\Pi \to a^3\Sigma$) as well as H_α and D_α lines were analyzed. The main conclusion is that in mixtures with D_2, dissociation of the D_2 is higher than dissociation of molecular hydrogen in mixtures with hydrogen. The absolute value of the continuum intensity is directly related to the rate of radiative dissociation via the $a^3\Sigma_g^+$ state and may be used for an estimation of the rate of H_2 dissociation by electron-impact. A comparison of intensities of the continuum spectrum and H (or D) atomic lines gives information about the dissociation degree of hydrogen or deuterium. As the input power is increased the intensity of continuum increases – i.e. the slope of the continuum rise. Therefore, the difference between deuterium and hydrogen continuum increases also with input power. This reveals that the difference between dissociation degree of deuterium and hydrogen increases with input power. An increase of dissociation level leads directly to an increase of intensity of excited atomic lines of H (or D). It may be expected that the ratio of atomic-hydrogen (deuterium) intensity to their molecular intensities will increase with dissociation level i.e. it should be larger for deuterium than for hydrogen. Data showed that the considered ratio for deuterium varies in the range 20-80 when in the hydrogen case is one order of magnitude smaller – which confirms more intensive dissociation for the case of mixture with deuterium. Figure 2 presents molecular H_2/D_2 and atomic excitation spectra.
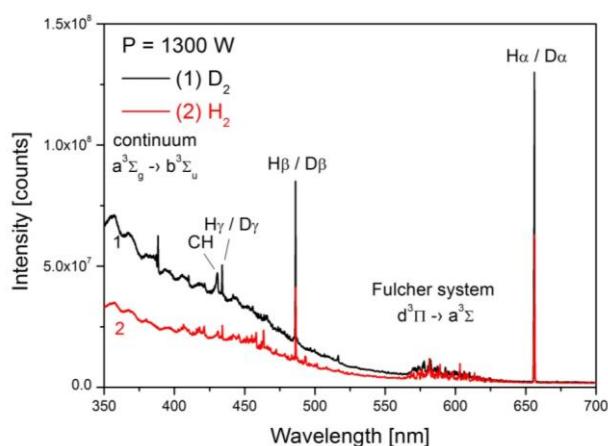

Figure 2. The emission of H_2 (D_2) Fulcher system ($d^3\Pi \to a^3\Sigma$), radiative-dissociation continuum ($a^3\Sigma_g \to b^3\Sigma_u$) as well as H_α and D_α lines for 1.3 kW microwave discharge; p = 6.7 kPa.

The most intensive part of the molecular spectra of H_2/D_2 is related to H_2 Fulcher-system emission ($d^3\Pi \to a^3\Sigma$) in the region 560 – 640 nm and continuous spectra in the region 220 – 550 nm.

6

The continuous spectrum is known as a radiative-dissociation continuum ($a^3\Sigma_g \rightarrow b^3\Sigma_u$), which results from the process:

$$H_2 \, (v = 0 \div m) + e \; \rightarrow H_2\left(a^3\Sigma_g^+\right) \; \rightarrow \; H_2(b^3\Sigma_u) \rightarrow 2H + h\nu \tag{1}$$
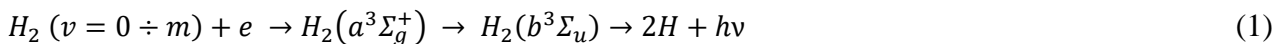
and corresponds to the main channel of the dissociation of H_2 in the discharge plasma.
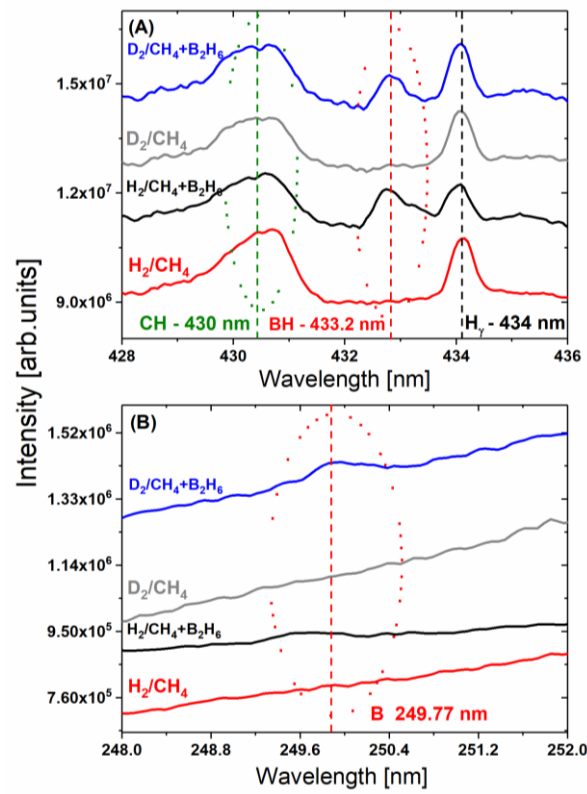

Figure 3. Emission spectral lines of CH, BH, H_y (A) and B species in H_2/CH$_4$ and D$_2$/CH$_4$ plasma (B) with and without the admixture of 10k ppm of B$_2$H$_6$.
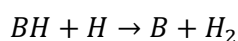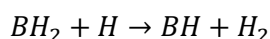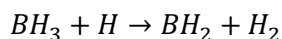
It can be seen that the hydrogen state H_β could be overexcited, i.e. the other process (not direct electron impact) could play an important role in its excitation. Only one process which can contribute to selective excitation of H_β -state is known - dissociative recombination:

$$H_2^+ + e^- = H(\beta) + H, \tag{2}$$

which appears as energetic resonance.

Differences in dissociation level of D$_2$ and H$_2$ are related most probably to differences in cross sections (CS) for the dissociation processes. From existing published data, CS for D$_2$ is slightly larger than for H$_2$ [24]. Besides, vibrational populations of H$_2$ and D$_2$ in-ground electronic states are important, because the vibrational levels may contribute to increased frequency of dissociation

7

processes. The admixture of small amount 5 - 10 ppm of B_2H_6 leads to a series of processes - see, e.g. [25]:

$$B_2H_6 \rightarrow BH_3 + BH_3 \quad - \text{ thermal dissociation} \tag{3}$$

$$BH_3 + H \rightarrow BH_2 + H_2$$

$$BH_2 + H \rightarrow BH + H_2$$

$$BH + H \rightarrow B + H_2$$

This leads to the appearance of features in the spectra related to BH and B emissions – the first is stronger. The oscillator strengths of BH_x (x>1) species are much smaller than BH, therefore it is problematic to observe them on the background of intensive hydrogen bands. The B emission (transition 3^2S->2^2P) appears approximately at 249.8 nm (Figure 3 (B)) and BH – 433 nm (Figure 3(A)). Strangely enough, the emission of B appears only in the case of mixtures with deuterium. There is not any data in the literature on this issue. However, details of this spectrum may result from differences in rate constants of the processes (3) or another mechanism of boron hydrides dissociation. The latter has been also suggested by Aubert et al. [26] basing on the measurements showing that the boron atoms prevail in colder regions. So, an additional possible mechanism with participation of excited and ionized species has been postulated, which can possibly explain the various roles of hydrogen/deuterium in quenching $B(2s^23s\ ^2S_{1/2})$ state as well.
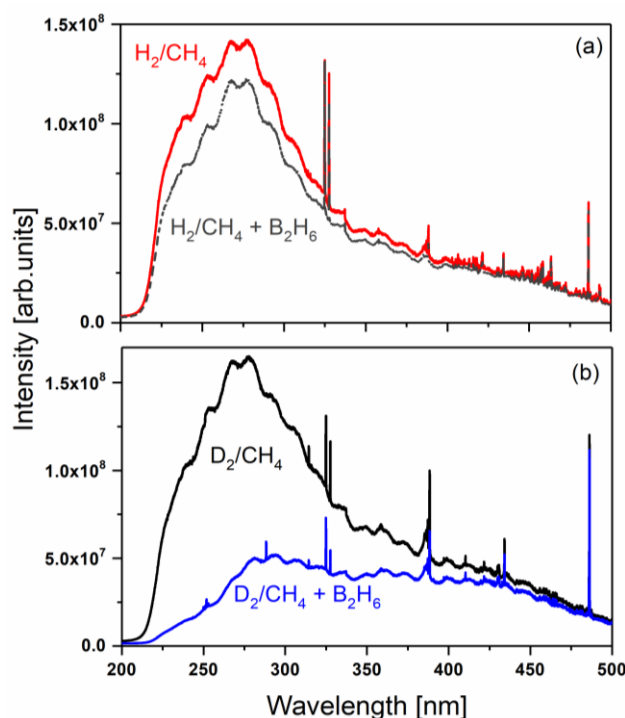
Figure 4. Emission spectra in the range 200-500 nm in (A) H_2/CH_4 and (B) D_2/CH_4 plasma both with and without the addition of 10k ppm of B_2H_6.

The second case is confirmed by following spectra details, mainly the addition of B_2H_6 leads to strong quenching of shortwave continuum (Figure 4(A)). This part of the spectrum corresponds to transitions (and dissociation) from low excited vibrational levels of D_2. The decrease of the continuum intensity, observed in the mixture of $D_2/CH_4+B_2H_6$ could be explained by quenching the vibrational D_2 molecule by B_2H_6 (Eq. 4). At the same time part corresponding to transitions from higher vibrationally excited D_2 does not change significantly - see spectral range above 400 nm in Fig. 4(B). It means that B_2H_6 can be involved in the quenching of low vibrational excited levels of D_2 i.e.

$$D_2(v > 0) + B_2H_6 \rightarrow D_2(v = 0) + B_2H_6(v'') \ , \tag{4}$$

which can increase $B_2H_6(v)$ dissociation (processes (3)) and boron production. These effects are not registered in the case of mixtures with hydrogen – see Fig. 4(A). The rate constant for D_2 is significantly larger than for H_2, what could be explained by smaller vibrational quantum for D_2 than H_2. The energy mismatch is high enough to dissociate B_2H_6.

3.2. The boron-doped diamond morphology and structure

The aim of LIBS measurements was to determine the boron doping level of BDD films synthesized in plasma with hydrogen or deuterium in the gas mixture. From the optical emission spectroscopy measurements carried out during CVD process, we have found that deuterium plasma can influence B_2H_6 dissociation process and lead to an increase of boron concentration in the plasma. LIBS emission spectra were recorded in time resolve mode in the spectral range 242 – 255 nm where the strongest boron lines 249.67 nm and 249.77 nm as well as weak carbon line 247.85 nm can be observed.
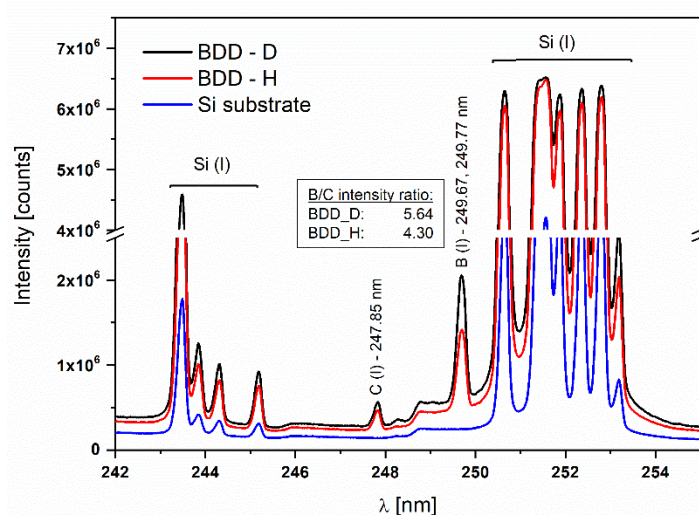
9

Figure 5. LIBS spectra recorded for BDD thin films synthesized in CVD process carried out in hydrogen or deuterium containing plasma.

The LIBS emission recorded for pure silicon substrate and covered with BDD film prepared in deuterium and hydrogen plasma are shown in Figure 5. The emission in the range of 243 – 246 nm and 250 - 254 nm originating from the silicon substrate. The relative boron concentration in BDD film was estimated from the B and C line intensity. The B/C intensity ratio for sample synthesized in deuterium plasma is 5.64 which is a higher value than in the case of film produced in hydrogen plasma – B/C = 4.30. This result confirmed that higher B_2H_6 dissociation level in deuterium plasma leads to higher boron concentration in BDD. All samples i.e. reference Si substrate as well as BDD_D and BBD_H films were analysed in the same conditions. Small differences in intensity observed in the LIBS signal recorded for BDD films originates probably from slight differences in film thickness.

Raman spectra recorded for BDD films prepared in deuterium and hydrogen plasma are presented in Figure 6. Except for the narrow sp^3 D-band at 1329 cm^{-1} and 1331 cm^{-1} the relatively intense sp^2 G-band centered at 1538 cm^{-1}, and 1540 cm^{-1} can be observed. In the range of 1000 to 1800 cm^{-1} a large amount of amorphous carbon can be seen, especially for BBD_H, which results in decrees of diamond line intensity due to optically dense of sp^2 carbon. It is well-known fact with increasing boron doping the crystallite size decrees and amount of polymeric sp^2 C at the grain boundaries increases. This phenomenon will affect electrical properties due to a small fraction of B atoms can be found in the small crystallites, so the majority of B atoms must be present at sites that do not contribute to the continuum of electronic states [27]. The lower amount of amorphous carbon in BDD_D sample can be explain by the extended dissociation and a higher rate of carbon species at the surface of growing film. The BDD_H sample also exhibits a wide band in the range of 2500 - 3000 cm^{-1} originating from CH stretching vibrations. The increased photoluminescence observed above 2000 cm^{-1} can also originate from nitrogen vacancy defects, however the characteristic NV0 emission peak at 575 nm expected to be seen at 2064 cm^{-1} in Raman shift scale for 514 nm excitation was not distinguishaed. The heavily boron influence reveals in the wideband near 1220 cm^{-1} for BDD_D were the Fano effect if visible [28]. Those bands can be attributed to lattice disorder and intra-band optical transitions caused by the presence of boron [47-49].
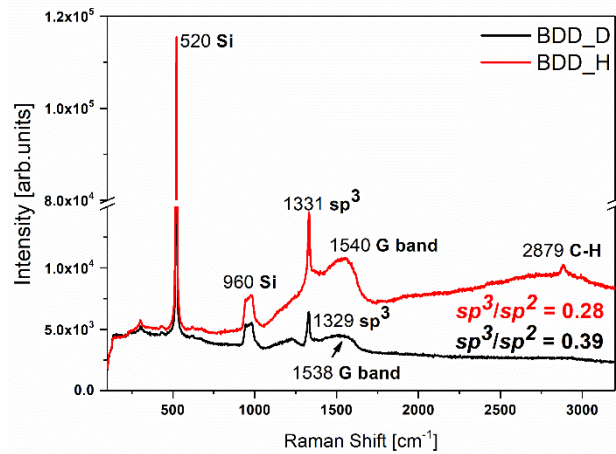
Figure 6. Raman spectra recorded for BDD thin films synthesized in CVD process carried out in hydrogen and deuterium

Figure 7 shows scanning electron microscope (SEM) images of boron-doped diamond films grown in deuterium and hydrogen-rich plasma taken with different magnification and artificially colored to enhance contrast and faceting of the crystal surface.
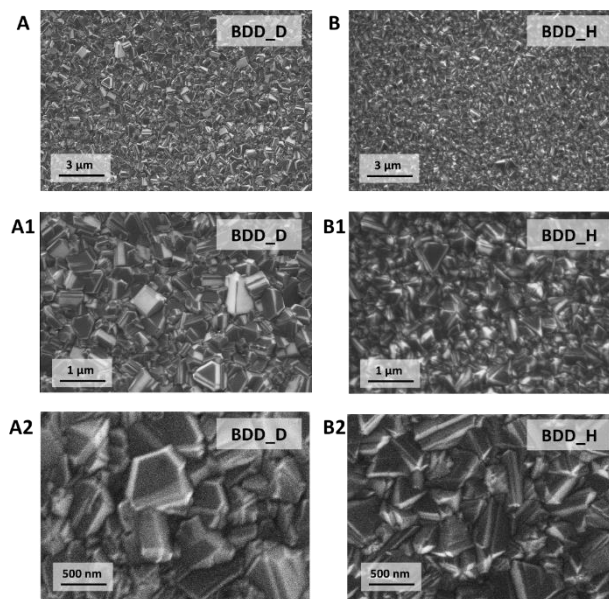

Figure 7. SEM micro-images of BDD_D (A, A1 and A2) and BDD_H (B, B1 and B2) surfaces (3 x 2 μm) taken with magnification of 5 000x, 10 000x and 50 000x.

It is well-known fact that boron doping has a significant impact on the morphology of film synthesized in hydrogen-based plasmas [29]. The high-resolution SEM images show that grains in BDD_D films are larger than the grains in BDD_H sample (see Figure 7A2 and 7B2). The edges of largest crystals have been marked by red color to illustrate qualitatively their contribution in hydrogen and deuterium deposited films. Ternyak *et al.* [19] have shown that the isotopic change of H to D in

the gas mixture influences the kinetics of diamond growth, but not its mechanism. Hence, it can be concluded that boron admixture has a minor impact on surface morphology in the case of BDD_D when compared to standard BDD films [30]. Furthermore, deuterium is responsible for the larger and more faceted grain, since the thermally activated deuterium tends to etch away defective grains and non-diamond species more effectively than hydrogen [20].

Higher doping efficiency for BDD_D sample is the result of higher energy (mass of D atom), and extended dissociation in the gas phase of gas species. Moreover, due to the higher energy, the rate of etching of carbon species at the growth plane is much higher than for hydrogen plasma. This result in a significantly fewer B atom in grains boundaries, and more in crystallites. Overall, the enhanced boron doping is attributed to the lower energy of B-H bond at the growth surface (389 kJ mol^{-1}), when compared to C-H bond (411 kJ mol^{-1}; one electron more). Thus, the hydrogen abstraction from B-H is dominant providing dangling bonds for diamond growth. This effect is enhanced by extended dissociation caused by deuterium rich plasma.

The growth rate of both BDD_H and BDD_D films was studied separately by spectroscopic ellipsometry and stylus profilometer and averaged. The deviation of thicknesses estimated by both methods was of the order of 10% (see Table 1). Comparing the film-growth rates in mixtures containing hydrogen (g$_{rate}$-H) and deuterium (g$_{rate}$-D), g$_{rate}$-H $\approx$ 2g$_{rate}$-D , indicate that the primary kinetic isotope effect is observed, i.e., the change of rate which occurs upon isotopic substitution of hydrogen by deuterium. The isotopic substitution (D for H) is a widely used tool for elucidating reaction mechanism. To a good approximation, the electronic structure of reagents, and thus carbon binding forces, remains the same. Any differences are attributable to the change in mass and manifest themselves primarily in the frequencies of vibrational modes of H and D atoms bonding. For our hypothetical growth model of a small H or D atom mass m attached to a much larger mass of bonded C atom by a spring of force constant k, the classical vibrational frequency is given by $v = \frac{1}{2\pi}\sqrt{\frac{k}{m}}$. The quantum mechanical treatment of the same model leads to energy levels $\varepsilon_n = (n+1/2)hv$, $n = 0, 1, 2,$ ... and thus energy- level separations $\Delta\varepsilon = hv$, where v is the classical frequency given above. Energies are measured from the lowest point on the potential energy surface. An important feature of the vibrational energy levels is that the energy of the lowest possible level lies ½(hv) above the minimum of the potential energy surface. From the classical equation for frequency v mentioned above this zero-point energy is inversely proportional to the square root of the atom mass. For this reason, the zero-point energy level stretching vibrations of C-H and C-D are different. The zero-point energy is proportional to v and thus to $\sqrt{1/m}$; the C-D bond, therefore, has lower zero-point energy than the C-

12

H bond, and greater activation energy is required for cleavage of the C-D bond. During the film-growth process, the C-H (C-D) bonds must break, so a primary isotope effect is observed. The stretching vibration of the reactants (H or D) is converted to the translational motion over the barrier between two energy minima on the potential energy hypersurface, and the zero-point energy disappears for that particular degree of freedom. Since the C-H degree of freedom starts out at a higher energy than C-D, its activation energy is lower, and g_{rate}-H / g_{rate}-D will be greater than 1.

We can calculate the isotope effect to be expected during film growth when the effect relative to zero-point energy is the only contributor. The C-D frequency should be smaller than the C-H frequency by a factor of roughly $1/\sqrt{2} = 1/1.4$. If we take this energy difference as being approximately equal to the difference in enthalpy of activation, we can use the Eyring equation to find the ratio of rate constants:

$$g_{rate} - H(-D) = \frac{kT}{h} exp\left(-\frac{\Delta H^{\#}}{RT}\right) exp\left(\frac{\Delta S^{\#}}{R}\right) \tag{5}$$

where T is reaction temperature in K, $\Delta H^{\#}$ is the difference in enthalpy of activation and $\Delta S^{\#}$ is entropy difference. We may assume that $\Delta S^{\#}$ will be equal for the two systems that differ only by substitution of H with D. After some algebra manipulations we obtain the known equation:

$$\frac{g_{rate}-H}{g_{rate}-D} \approx exp\left(\frac{0.2055}{T}V_H\right), \tag{6}$$

where v_H is the energy of C-H stretching vibration in cm^{-1}. The C-H stretching vibration appears in the infrared spectrum around 3000 cm^{-1} and is not strongly temperature dependent so approximately can be treated as constant, and finally, we have $\frac{g_{rate}-H}{g_{rate}-D} \approx exp\left(\frac{0.616.6}{T}\right)$. The H/D isotope effect at T = 298 K would therefore equal 7.9. Note however, that the isotope effect is larger the lower the temperature. If we take experimentally observed (see Table 1) g_{rate}-H/g_{rate}-D $\approx 4.05/1.79 = 2.26$ then the temperature of the diamond-surface growth can be estimated as 500°C, about 200°C lower than one set during the process.

Table 1. Thickness and growth kinetics of BDD samples grown by hydrogen or deuterium-based plasma

| Sample	Growth time (min)	Film thickness (nm)	Growth rate (nm min^{-1})
BDD_H	60	243	4.05
BDD_D	**120**	**215**	**1.79**

13

The influence of deuterium admixture is comparable with observations reported in [31–33]. The substitution of hydrogen by deuterium flow has more than halved the growth rate of boron-doped diamond films, i.e., deuterium changed it from ~4 nm min^{-1} for hydrogen to 1.8 nm min^{-1}.

The kinetic isotope effect, a change of reaction rate that occurs upon isotopic substitution, is widely used as a tool for elucidating reaction mechanism. When diamond thin-film growth in H_2/D_2 microwave plasma-assisted CVD process is compared, the growth in deuterium is about twice as slow in comparison with hydrogen. Since hydrogen or deuterium termination of diamond surfaces is important regarding stabilizing the surface (and hence the bulk diamond) structure against the phase transition, we assume that the sample surface is almost perfectly hydrogenated or deuterated during the whole growth process.

So g_{rate}-H/g_{rate}-D ≈ 2 shows that the removal of the hydrogen from a surface is a slow, rate-determining step. Since the plasma used for diamond thin-film synthesis contains mainly hydrogen or deuterium with just a few percents of methane, the H_2, H, and H^+ or D_2, D and D^+ species are the dominant ones. However, provided that the reactivity of H_2 and D_2 are relatively low in comparison with the rest, we have considered only H, D, and H^+, D^+. The reactivity of cationic species of hydrogen and deuterium are low for thermodynamic reasons since reactions

$$^1C_{(S)}\text{-H(D)} + H^+(D^+) = {}^2C_{(S)} + {}^2H_2^+({}^2D_2^+), \quad \Delta H_0 = 0.71 \text{ eV}, \tag{7}$$
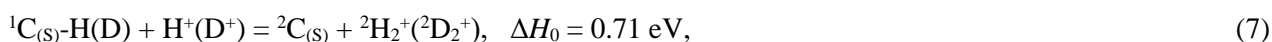
are substantially endothermic although with low activation energy. The other possible reaction

$$^1C_{(S)}\text{-H(D)} + {}^2H({}^2D) = {}^2C_{(S)} + {}^1H_2({}^1D_2), \quad \Delta H_0 = -0.98 \text{ eV}, \tag{8}$$
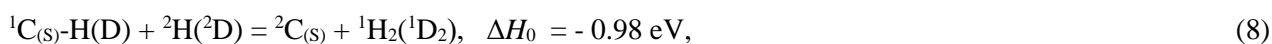
is in perfect agreement with the observed kinetic isotopic effect. The last considered reaction produces the reactive radical-dangling bonds, $^2C_{(S)}$, on the diamond surface which reacts with very diluted carbon species from plasma such as $^2CH_4^+$ ($^2CD_4^+$), $^1CH_3^+$ ($^1CD_3^+$), $^2CH_2^+$ ($^2CD_2^+$), $^1CH^+$ ($^1CD^+$), $^2C^+$ as well as $^2CH_3$ ($^2CD_3$), $^1CH_2$ (CD_2), ^2CH (^2CD) or its higher excited states. Reactivity of boron species with surface radical-dangling bonds are very similar, but as the [B]/[C] ratio in the gas phase is very low, the B_2H_6 influence on the measured reaction rate is not significant.

Similar growth rates of BDD_H films have already been reported for fused silica [34–36] or silicon substrates [30,37]. It is worth noting that the deuterium-based plasma impairs growth kinetics mainly due to the more intensive etching of non-diamond forms. This is mainly attributed to larger kinetic energies of deuterium atoms as well as extended diffusion coefficients of deuterium in the BDD films and interaction with negatively charged boron acceptors. In comparison, the growth rate of deuterium diamond films grown in HFCVD is known to be ~3 times slower than that of films grown

14

from hydrogen-based plasma for undoped samples [32,33]. Additionally, the MW PACVD process slows down approx. 2 times, when *in-situ* boron-doping films are applied (e.g., diborane precursor admixture) [38].

3.3. The electronic and optical properties of boron-doped diamond films

Next, Hall mobility and 4-point probe studies have been performed to reveal the activation of incorporated boron in the diamond films. The electronic properties have been listed in Table 2. The higher incorporation of boron in the BDD_D film shown by LIBS is also proved by the higher charge carrier density. At room temperature, the BDD sample grown in a mixture containing hydrogen has a hole concentration of 1.51×10^{19} atoms cm^{-3}, while in BDD_D films the carrier concentration increases up to $1.28 \ 10^{20}$ atoms cm^{-3}. The BDD_D films show lower resistance of 0.25 Ohm·cm, which could be attributed to the direct carrier transfer along the large grains and tunneling in the intergrain regions. It was reported by Habka et al. [29] that the grain size of the polycrystalline diamond is the key parameter for efficient deuterium diffusion and trapping on boron atoms. The boron impurity centers induce the formation of an impurity band (with a bandwidth of ~0.2 eV for a boron concentration of $\sim 10^{19} \ cm^{-3}$) and hopping conduction through nearest-neighbors takes place [39]. The polarity of Hall voltage indicates that holes are free carriers in all the samples and both deuterium and hydrogen grown boron-doped diamond films demonstrated p-type conduction.

Table 2. Electronic properties of hydrogen (BDD_H) and deuterium (BDD_D) plasma deposited samples.

Sample	Charge carrier density (acceptors cm⁻³)	Hall mobility (cm² V⁻¹s⁻¹)	Resistance (Ohm cm)
BDD_H	1.51×10^{19}	4.06	15.38
BDD_D	**1.28×10^{20}**	**0.47**	**0.25**

The ellipsometric parameters Ψ and Δ were measured at room temperature for a 70° angle of incidence in the wavelength range from 260 to 830 nm. A four-layer structural model (ambient/BDD/Si wafer – substrate) was applied to describe the samples in order to determine the thickness of BDD film and its effective complex dielectric function. The diamond film has been assumed to be isotropic, homogeneous material. The dielectric function was fitted to the Tauc-Lorentz oscillator model using the non-linear Levenberg - Marquardt regression method and mean-square error of minimization [40]. As a result of SE analysis, the thickness and optical constants, i.e., refractive index $n(\lambda)$ and extinction coefficient $k(\lambda)$ were determined.

15

Figure 8 illustrates the spectral variation of n(λ) and k(λ) for boron-doped diamond films deposited in deuterium and hydrogen-rich plasma. Both deposited diamond films show the normal dispersion of refractive index in the studied wavelength range. The single crystal diamond refractive index has been plotted as a reference [41]. The achieved values of *n* were high, ranging from 2.35 to 2.55 for BDD_D films deposited in deuterium rich plasma (Figure 8). They are slightly larger than those estimated for BDD_H films, which is consistent with a highly faceted crystal structure in SEM and the larger sp^3/sp^2 ratio revealed by Raman. Moreover, index *n* of BDD_D, when compared to single crystal diamond, indicates a slightly lower physical and optical density [42,43]. The *n* - values between 2.31 and 2.34 were reported by Hu *et al.* [44,45] for undoped nanocrystalline diamond films or 1.7-2.1 by Gupta *et al.* [46] for microcrystalline diamond films at *λ*= 632 nm. Recent results [47] have shown that boron-doped diamond films possess lower values of refractive index (2.4 @550 nm) than those observed here for BDD_D. Generally, the boron incorporation in the BDD structure decreases the refractive index inducing more C-H defects, boron clusters, sp^2 hybridized phases as revealed by Raman studies (pronounced "G" band in Figure 6).
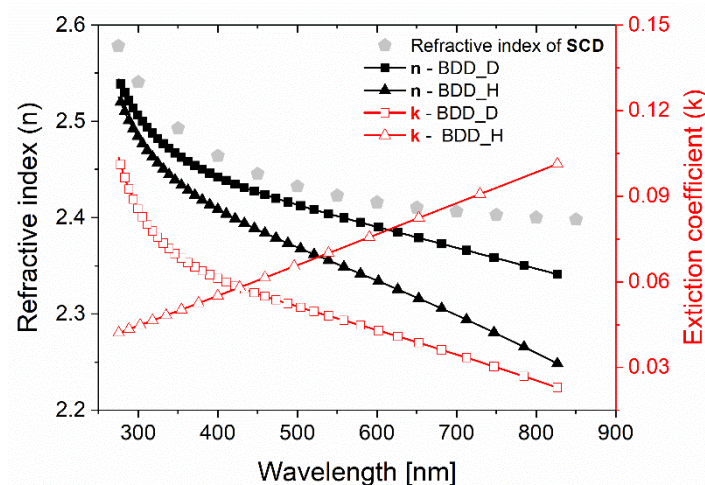

Figure 8. Variation of optical constants (*n(λ)* and *k(λ)*) of boron-doped diamond films grown using hydrogen (BDD_H) or deuterium (BDD_D) rich plasma.

Figure 8 also illustrates *k*-values of BDD_D, which exhibit the opposite slope to that estimated for BDD_H. Nevertheless, both BDD_H and BDD_D present a similar range of extinction-coefficient variation from 0.03 to 0.1 in the VIS range. The abnormal character of extinction plot should be attributed to boron acceptor incorporation. The high boron doped films exhibit such a character due to the energy of the absorption line ~ 0.29 eV, which is close to the boron acceptor level (0.38 eV) formed during the incorporation of the B atoms in a diamond lattice [48]. A similar phenomenon was also described by other works focused on BDD [49–51].

16

4. Conclusions

Summarizing, boron-doped diamond films were grown in a deuterium-rich gas mixture, BDD_D. It was shown that the deuterium is the key parameter influencing growth kinetics and modifying mechanism of boron incorporation. Observed properties are thermally and electron-driven, leading to increased radical generation and modified chemistry towards improved boron-doped diamond quality and enhanced efficiency of boron doping. The optical and electrical properties of diamond samples grown in hydrogen and deuterium rich gas mixtures were studied and compared. The boron activation is evidenced by the increase in the carrier concentration and the decrease in the Hall mobility for the BDD_D samples.

LIBS results revealed that more boron is incorporated in diamond films when deposited with deuterium rich plasma. Lower concentrations of sp^2 phases and C-H defects have been noticed in the BDD_D in relation to BDD_H. Also, sp^3 diamond peak is shifted more to the left, which is mostly attributed to the larger boron doping. The Fano effect is also here pronounced at 1220 cm^{-2}, which confirms LIBS results.

It is well known that diffusion of deuterium in boron-doped diamond results in the passivation of boron acceptors with the formation of (B-D) complexes impairing B-B and B-H impurities development. At low power density, the electron processes would appear to be necessary to describe the diborane dissociation. The BH$_3$ density was previously correlated with the doping process evolution [52], and thus BH$_3$ appears as the most probable boron species responsible for doping. It is recognized as an effective source of boron atoms [53] but not as final active specie. Moreover, Cheesman *et al.* [54] reported that BH$_x$ (x = 0–3) species can all bind to radical sites on the diamond {100} surface to form stable complexes.

The enhanced boron doping is attributed to the lower energy of B-H bond at the growth surface, when compared to C-H bond (one electron more). In such a case, the hydrogen abstraction from B-H site is providing dangling bonds for diamond growth. This effect plays a main role due to extended dissociation caused by deuterium rich plasma. A strong influence of the B-H in causing the boron incorporation level in diamond lattice is confirmed by the correlation of its modeled equilibrium composition in the gas phase with boron content as determined experimentally by LIBS or Raman spectroscopy.

17

References

[1] Asmussen/Reinha, D.K. Reinhard, Diamond Films Handbook, CRC Press, 2002.

[2] C. Nebel, ed., Thin-Film Diamond II, Volume 77:, Academic Press, Amsterdam; Boston, 2004.

[3] R.F. Davis, Diamond films and coatings development, properties, and applications, Noyes Pub., Park Ridge, N.J., 1993.

[4] N. Yang, ed., Novel Aspects of Diamond, Springer International Publishing, Cham, 2015. http://link.springer.com/10.1007/978-3-319-09834-0 (accessed October 10, 2015).

[5] A. Suzuki, T.A. Ivandini, K. Yoshimi, A. Fujishima, G. Oyama, T. Nakazato, N. Hattori, S. Kitazawa, Y. Einaga, Fabrication, Characterization, and Application of Boron-Doped Diamond Microelectrodes for in Vivo Dopamine Detection, Anal. Chem. 79 (2007) 8608–8615. doi:10.1021/ac071519h.

[6] G.M. Swain, The use of CVD diamond thin films in electrochemical systems, Adv. Mater. 6 (1994) 388–392. doi:10.1002/adma.19940060511.

[7] T. Klein, P. Achatz, J. Kacmarcik, C. Marcenat, F. Gustafsson, J. Marcus, E. Bustarret, J. Pernot, F. Omnes, B.E. Sernelius, C. Persson, A. Ferreira da Silva, C. Cytermann, Metal-insulator transition and superconductivity in boron-doped diamond, Phys. Rev. B. 75 (2007) 165313. doi:10.1103/PhysRevB.75.165313.

[8] A. Kawano, H. Ishiwata, S. Iriyama, R. Okada, T. Yamaguchi, Y. Takano, H. Kawarada, Superconductor-to-insulator transition in boron-doped diamond films grown using chemical vapor deposition, Phys. Rev. B. 82 (2010) 085318. doi:10.1103/PhysRevB.82.085318.

[9] J. Bousquet, T. Klein, M. Solana, L. Saminadayar, C. Marcenat, E. Bustarret, Phase diagram of boron-doped diamond revisited by thickness-dependent transport studies, Phys. Rev. B. 95 (2017) 161301. doi:10.1103/PhysRevB.95.161301.

[10] S. Wang, V.M. Swope, J.E. Butler, T. Feygelson, G.M. Swain, The structural and electrochemical properties of boron-doped nanocrystalline diamond thin-film electrodes grown from Ar-rich and H2-rich source gases, Diam. Relat. Mater. 18 (2009) 669–677. doi:10.1016/j.diamond.2008.11.033.

[11] R. Issaoui, J. Achard, F. Silva, A. Tallaire, A. Tardieu, A. Gicquel, M.A. Pinault, F. Jomard, Growth of thick heavily boron-doped diamond single crystals: Effect of microwave power density, Appl. Phys. Lett. 97 (2010) 182101. doi:10.1063/1.3511449.

[12] T. Teraji, H. Wada, M. Yamamoto, K. Arima, T. Ito, Highly efficient doping of boron into high-quality homoepitaxial diamond films, Diam. Relat. Mater. 15 (2006) 602–606. doi:10.1016/j.diamond.2006.01.011.

[13] J. Chevallier, F. Jomard, Z. Teukam, S. Koizumi, H. Kanda, Y. Sato, A. Deneuville, M. Bernard, Hydrogen in n-type diamond, Diam. Relat. Mater. 11 (2002) 1566–1571. doi:10.1016/S0925-9635(02)00063-8.

[14] K.M. Rutledge, K.K. Gleason, Hydrogen in Cvd Diamond Films, Chem. Vap. Depos. 2 (1996) 37–43. doi:10.1002/cvde.19960020203.

[15] R. Bogdanowicz, A. Fabiańska, L. Golunski, M. Sobaszek, M. Gnyba, J. Ryl, K. Darowicki, T. Ossowski, S.D. Janssens, K. Haenen, E.M. Siedlecka, Influence of the boron doping level on the electrochemical oxidation of the azo dyes at Si/BDD thin film electrodes, Diam. Relat. Mater. 39 (2013) 82–88. doi:10.1016/j.diamond.2013.08.004.

[16] D. Ballutaud, F. Jomard, B. Theys, C. Mer, D. Tromson, P. Bergonzo, Hydrogen diffusion and stability in polycrystalline CVD undoped diamond, Diam. Relat. Mater. 10 (2001) 405–410. doi:10.1016/S0925-9635(00)00590-2.

[17] J. Chevallier, B. Theys, A. Lusson, C. Grattepain, A. Deneuville, E. Gheeraert, Hydrogen-boron interactions in p-type diamond, Phys. Rev. B. 58 (1998) 7966–7969. doi:10.1103/PhysRevB.58.7966.

[18] N. Mizuochi, J. Isoya, J. Niitsuma, T. Sekiguchi, H. Watanabe, H. Kato, T. Makino, H. Okushi, S. Yamasaki, Isotope effects between hydrogen and deuterium microwave plasmas on chemical vapor deposition homoepitaxial diamond growth, J. Appl. Phys. 101 (2007) 103501. doi:10.1063/1.2727380.

[19] O. Ternyak, S. Michaelson, L. Tkach, R. Akhvlediani, A. Hoffman, The impact of gas isotopic exchange on the growth rate and hydrogen (deuterium) bonding within CVD diamond films, Phys. Status Solidi A. 204 (2007) 2839–2846. doi:10.1002/pssa.200776303.

[20] I.Y. Koenka, A. Stacey, R. Akhvlediani, S. Prawer, A. Hoffman, The impact of H/D substitution on the structure, composition and thermal stability of grain boundaries in sub-micron diamond films deposited on silicon, Diam. Relat. Mater. 22 (2012) 59–65. doi:10.1016/j.diamond.2011.11.008.

[21] J. Chevallier, B. Theys, A. Lusson, C. Grattepain, A. Deneuville, E. Gheeraert, Hydrogen-boron interactions in p-type diamond, Phys. Rev. B. 58 (1998) 7966–7969. doi:10.1103/PhysRevB.58.7966.

[22] J. Chevallier, A. Lusson, D. Ballutaud, B. Theys, F. Jomard, A. Deneuville, M. Bernard, E. Gheeraert, E. Bustarret, Hydrogen-acceptor interactions in diamond, Diam. Relat. Mater. 10 (2001) 399–404. doi:10.1016/S0925-9635(00)00432-5.

[23] N. Habka, E. Chikoidze, F. Jomard, Y. Dumont, J. Chevallier, J. Barjon, C. Mer, P. Bergonzo, Deuterium-induced passivation of boron acceptors in polycrystalline diamond, J. Appl. Phys. 108 (2010) 123701. doi:10.1063/1.3518608.

[24] J.-S. Yoon, Y.-W. Kim, D.-C. Kwon, M.-Y. Song, W.-S. Chang, C.-G. Kim, Vijay Kumar, B. Lee, Electron-impact cross sections for deuterated hydrogen and deuterium molecules, Rep. Prog. Phys. 73 (2010) 116401. doi:10.1088/0034-4885/73/11/116401.

[25] J. Ma, J.C. Richley, D.R.W. Davies, M.N.R. Ashfold, Y.A. Mankelevich, Spectroscopic and Modeling Investigations of the Gas Phase Chemistry and Composition in Microwave Plasma Activated B2H6/CH4/Ar/H2 Mixtures, J. Phys. Chem. A. 114 (2010) 10076–10089. doi:10.1021/jp104532y.

[26] X. Aubert, C.Y. Duluard, N. Sadeghi, A. Gicquel, Comparison of three optical diagnostic techniques for the measurement of boron atom density in a H2/B2H6 microwave plasma, Plasma Sources Sci. Technol. 26 (2017) 115011. doi:10.1088/1361-6595/aa94d8.

[27] P.W. May, W.J. Ludlow, M. Hannaway, P.J. Heard, J.A. Smith, K.N. Rosser, Raman and conductivity studies of boron-doped microcrystalline diamond, facetted nanocrystalline diamond and cauliflower diamond films, Diam. Relat. Mater. 17 (2008) 105–117. doi:10.1016/j.diamond.2007.11.005.

[28] J.W. Ager, W. Walukiewicz, M. McCluskey, M.A. Plano, M.I. Landstrass, Fano interference of the Raman phonon in heavily boron-doped diamond films grown by chemical vapor deposition, Appl. Phys. Lett. 66 (1995) 616–618. doi:10.1063/1.114031.

[29] X.Z. Liao, R.J. Zhang, C.S. Lee, S.T. Lee, Y.W. Lam, The influence of boron doping on the structure and characteristics of diamond thin films, Diam. Relat. Mater. 6 (1997) 521–525. doi:10.1016/S0925-9635(96)00640-1.

[30] R. Bogdanowicz, A. Fabianska, L. Golunski, M. Sobaszek, M. Gnyba, J. Ryl, K. Darowicki, T. Ossowski, S.D. Janssens, K. Haenen, E.M. Siedlecka, Influence of the boron doping level on the electrochemical oxidation of the azo dyes at Si/BDD thin film electrodes, Diam. Relat. Mater. 39 (2013) 82–88. doi:10.1016/j.diamond.2013.08.004.

[31] T. Teraji, H. Wada, M. Yamamoto, K. Arima, T. Ito, Highly efficient doping of boron into high-quality homoepitaxial diamond films, Diam. Relat. Mater. 15 (2006) 602–606. doi:10.1016/j.diamond.2006.01.011.

[32] O. Ternyak, S. Michaelson, L. Tkach, R. Akhvlediani, A. Hoffman, The impact of gas isotopic exchange on the growth rate and hydrogen (deuterium) bonding within CVD diamond films, Phys. Status Solidi A. 204 (2007) 2839–2846. doi:10.1002/pssa.200776303.

[33] I.Y. Koenka, A. Stacey, R. Akhvlediani, S. Prawer, A. Hoffman, The impact of H/D substitution on the structure, composition and thermal stability of grain boundaries in sub-micron diamond films deposited on silicon, Diam. Relat. Mater. 22 (2012) 59–65. doi:10.1016/j.diamond.2011.11.008.

[34] Michal Sobaszek Robert Bogdanowicz, Improved surface coverage of an optical fibre with nanocrystalline diamond by the application of dip-coating seeding, Diam. Relat. Mater. 55 (2015) 52–63. doi:10.1016/j.diamond.2015.03.007.

[35] M. Sobaszek, Ł. Skowroński, R. Bogdanowicz, K. Siuzdak, A. Cirocka, P. Zięba, M. Gnyba, M. Naparty, Ł. Gołuński, P. Płotka, Optical and electrical properties of ultrathin transparent nanocrystalline boron-doped diamond electrodes, Opt. Mater. 42 (2015) 24–34. doi:10.1016/j.optmat.2014.12.014.

[36] R. Bogdanowicz, Characterization of optical and electrical properties of transparent conductive boron-doped diamond thin films grown on fused silica, Metrol. Meas. Syst. 21 (2014) 685–698.

[37] R. Bogdanowicz, M. Sobaszek, J. Ryl, M. Gnyba, M. Ficek, Ł. Gołuński, W.J. Bock, M. Śmietana, K. Darowicki, Improved surface coverage of an optical fibre with nanocrystalline diamond by the application of dip-coating seeding, Diam. Relat. Mater. 55 (2015) 52–63. doi:10.1016/j.diamond.2015.03.007.

[38] X.H. Wang, G.-H.M. Ma, W. Zhu, J.T. Glass, L. Bergman, K.F. Turner, R.J. Nemanich, Effects of boron doping on the surface morphology and structural imperfections of diamond films, Diam. Relat. Mater. 1 (1992) 828–835. doi:10.1016/0925-9635(92)90109-2.

[39] K.E. Bennet, K.H. Lee, J.N. Kruchowski, S.-Y. Chang, M.P. Marsh, A.A. Van Orsow, A. Paez, F.S. Manciu, Development of Conductive Boron-Doped Diamond Electrode: A microscopic, Spectroscopic, and Voltammetric Study, Materials. 6 (2013) 5726–5741. doi:10.3390/ma6125726.

[40] H.G. Tompkins, E.A. Irene, eds., Handbook of ellipsometry, William Andrew Pub. ; Springer, Norwich, NY : Heidelberg, Germany, 2005.

[41] Asmussen/Reinha, D.K. Reinhard, Diamond Films Handbook, CRC Press, 2002.

[42] J. Robertson, Diamond-like amorphous carbon, Mater. Sci. Eng. R Rep. 37 (2002) 129–281. doi:10.1016/S0927-796X(02)00005-0.

[43] G. Davies, Properties and growth of diamond, INSPEC, the Institution of Electrical Engineers, 1994.

[44] Z.G. Hu, P. Hess, Optical constants and thermo-optic coefficients of nanocrystalline diamond films at 30–500 °C, Appl. Phys. Lett. 89 (2006) 081906-081906–3. doi:doi:10.1063/1.2243863.

[45] Z.G. Hu, P. Prunici, P. Hess, K.H. Chen, Optical properties of nanocrystalline diamond films from mid-infrared to ultraviolet using reflectometry and ellipsometry, J. Mater. Sci. Mater. Electron. 18 (2007) 37–41. doi:10.1007/s10854-007-9175-y.

[46] S. Gupta, B.R. Weiner, G. Morell, Ex situ spectroscopic ellipsometry investigation of the layered structure of polycrystalline diamond thin films grown by electron cyclotron resonance-assisted chemical vapor deposition, J. Appl. Phys. 90 (2001) 1280–1285. doi:doi:10.1063/1.1384487.

[47] M. Ficek, M. Sobaszek, M. Gnyba, J. Ryl, Ł. Gołuński, M. Smietana, J. Jasiński, P. Caban, R. Bogdanowicz, Optical and electrical properties of boron doped diamond thin conductive films deposited on fused silica glass substrates, Appl. Surf. Sci. 387 (2016) 846–856. doi:10.1016/j.apsusc.2016.06.165.

[48] M. Sobaszek, Ł. Skowroński, R. Bogdanowicz, K. Siuzdak, A. Cirocka, P. Zięba, M. Gnyba, M. Naparty, Ł. Gołuński, P. Płotka, Optical and electrical properties of ultrathin transparent nanocrystalline boron-doped diamond electrodes, Opt. Mater. 42 (2015) 24–34. doi:10.1016/j.optmat.2014.12.014.

[49] J. Nakamura, E. Kabasawa, N. Yamada, Y. Einaga, D. Saito, H. Isshiki, S. Yugo, R.C.C. Perera, Electronic structures of B2p and C2p levels in boron-doped diamond films studied using soft x-ray absorption and emission spectroscopy, Phys. Rev. B. 70 (2004) 245111. doi:10.1103/PhysRevB.70.245111.

[50] W. Gajewski, P. Achatz, O.A. Williams, K. Haenen, E. Bustarret, M. Stutzmann, J.A. Garrido, Electronic and optical properties of boron-doped nanocrystalline diamond films, Phys. Rev. B. 79 (2009) 045206. doi:10.1103/PhysRevB.79.045206.

[51] D. Wu, Y.C. Ma, Z.L. Wang, Q. Luo, C.Z. Gu, N.L. Wang, C.Y. Li, X.Y. Lu, Z.S. Jin, Optical properties of boron-doped diamond, Phys. Rev. B. 73 (2006) 012501. doi:10.1103/PhysRevB.73.012501.

[52] C. Rond, R. Salem, S. Hamann, G. Lombardi, J. Röpcke, A. Gicquel, Chemical analysis of H2–B2H6and H2–CH4–B2H6microwave CVD plasmas used for diamond deposition, Plasma Sources Sci. Technol. 25 (2016) 025016. doi:10.1088/0963-0252/25/2/025016.

[53] Q. Liang, J.G. Harrison, Y.K. Vohra, Modeling of nitrogen/diborane/methane/hydrogen plasma for nanocrystalline diamond growth: Comparison with experimental data, Diam. Relat. Mater. 17 (2008) 2067–2070. doi:10.1016/j.diamond.2008.07.001.

[54] A. Cheesman, J.N. Harvey, M.N.R. Ashfold, Computational studies of elementary steps relating to boron doping during diamond chemical vapour deposition, Phys. Chem. Chem. Phys. 7 (2005) 1121–1126. doi:10.1039/B418664H.